L-edge x-ray absorption fine structure study of growth and morphology of ultrathin nickel films deposited on copper

Robert Nietubyć, Alexander Föhlisch, Leif Glaser, Julian Tobias Lau, Michael Martins, Matthias Reif, and Wilfried Wurth
University of Hamburg, Institute of Experimental Physics, Luruper Chaussee 149, D-22761 Hamburg, Germany
(Received 1 October 2003; revised manuscript received 3 March 2004; published 14 December 2004)

We have studied the Ni *L* edge x-ray absorption fine structure for thin Ni films evaporated on a Cu(001) substrate. The measurements have been carried out for films having coverages ranging from 0.07 monolayers (ML) up to 3.1 ML. The coverage has been calibrated using the ratio of the Ni L_3 to Cu L_3 edge jump heights and independently verified with titration experiments. We have found a clear evolution of the x-ray absorption fine structure at the Ni L_3 edge with coverage. To interpret the measured spectra first-principles calculations have been performed modeling a two-dimensional growth. The calculations reproduced all features observed experimentally. From the comparison between experiment and theory we can conclude that submonolayer films contain a large number of small islands. Deposition of an amount of nickel corresponding to a single layer results in the formation of an almost perfect flat layer. Our studies show that *L* edge x-ray absorption spectroscopy can provide useful information on thin-film growth and morphology.

DOI: 10.1103/PhysRevB.70.235414 PACS number(s): 68.55.Ac, 61.10.Ht

I. INTRODUCTION

Layered structures give the possibility to study phenomena typical for objects of lowered dimensionality, absent or inaccessible in bulk materials. The understanding of the magnetic, electronic, chemical, and mechanical properties of layered structures, which are often promising from a technological point of view, requires the knowledge of the growth properties and the resulting geometric and electronic structure. The structure of thin films Ni on Cu(001), has been widely studied theoretically[1–3] and experimentally using low energy electron diffraction (LEED) (Refs. 4 and 5) and scanning tunnel microscopy (STM) (Refs. 6 and 7) in order to explain its interesting magnetic properties, in particular out of plane magnetization,[8] in terms of crystalline structure and morphology. The present paper proposes a spectroscopic method of structural investigation for these films using x-ray absorption spectroscopy with synchrotron radiation.

In an x-ray absorption experiment the photon energy can be tuned selectively to an absorption edge which corresponds to atoms constituting the evaporated film. The structural information contained in the x-ray absorption fine structure is therefore limited to the local environment of the respective atoms in the film. Further enhancement of the structural information coming from the evaporated film is possible using primary beam polarization parallel to the surface (normal incidence).

L edge x-ray absorption near edge fine structure (NEXAFS) spectroscopy has been successfully used to study unoccupied electronic states above the Fermi level for thin Ni/Cu(001) (Ref. 9) and Cu/Ni(001) (Ref. 10) films. The geometric structure of 5–10 ML (ML—monolayers) thick Ni/Cu(001) films has been studied with *K* edge extended x-ray absorption fine structure (EXAFS).[11] In the present paper we demonstrate the use of *L* edge absorption data to obtain structural information on the growth of nickel layers on a Cu(001) substrate. We analyze Ni L_3-absorption fine structure up to 60 eV above the L_2 edge in order to trace the process of island nucleation, aggregation, and coalescence. Experimental results are compared to *ab initio* calculations. We interpret the shape of the spectrum in terms of contributions provided by different Ni sites.

II. EXPERIMENTAL

Ni films have been prepared in an UHV chamber at a base pressure of 5×10^{-10} mbar. Prior to deposition the copper crystal was cleaned using standard procedures of cycles of Ar^+ sputtering followed by annealing to 900 K. Nickel was evaporated at room temperature from a 50 μm foil heated with 32 A dc current resulting in a deposition rate of 0.133 ± 0.006 ML/min. After deposition the sample was annealed at 400 K by 2 min in order to reduce the surface roughness. The complete description of the UHV chamber and nickel film preparation procedure has been presented in Ref. 12.

We have prepared 19 different nickel films in a coverage range from 0.07 to 3.1 ML. Additionally, we have prepared a "bulk" nickel sample obtained by deposition of a nickel film which was thicker than 30 ML. The Ni $L_{2,3}$ edge x-ray absorption total electron yield spectra have been measured in a sample current mode at the beamline BW3 at the DORIS storage ring at HASYLAB. The undulator radiation has been monochromatized with a SX700 monochromator using a 1220 l/mm gold coated plane grating, the exit slit width was set to 100 μm. The resulting photon energy bandwidth was 0.5 eV at 852 eV (Ni L_3 edge). The primary beam intensity was monitored with a molybdenum grid. The normal incidence absorption spectra have been measured in a photon energy range from 840 eV up to 970 eV with a step width of 0.2 eV and a time of measurement of 4 s per point. These parameters enabled a complete energy scan without a significant sample contamination due to residual gas adsorption. Except for the two thickest films, at least two samples have been prepared and measured for each coverage. Spectra mea-

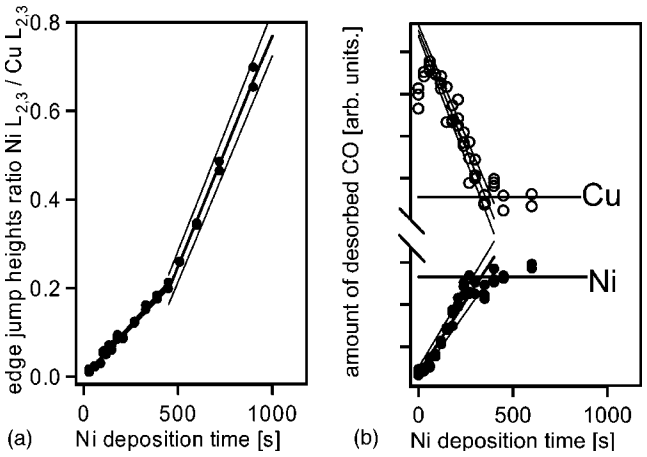

FIG. 1. (a)—Ratio of Ni $L_{2,3}$ to Cu $L_{2,3}$ absorption edge jump heights as a function of Ni deposition time. (b)—integrated intensities of the thermal desorption spectroscopy maxima corresponding to CO desorption from Cu (open dots) and Ni (solid dots) surfaces as a function of Ni deposition time. Horizontal lines show a zero level for copper and saturation level for Ni, respectively. Points are shifted apart vertically for better visualization.

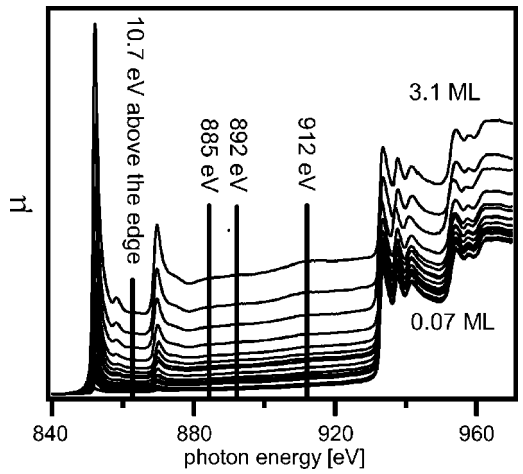

FIG. 2. Experimental x-ray absorption spectra results for all considered coverages. Spectra are normalized to the Cu $L_{2,3}$ edge absorption jump height.

sured for the same coverage have been summed up after checking the reproducibility.

The coverage has been estimated from the ratio of the edge jump height at the nickel absorption edge to the edge jump height at the copper edge. Figure 1(a) shows this ratio plotted versus deposition time. Two different linear functions have been fitted to the experimental values in two deposition time regions. A distinct increase of the slope after a deposition time of 450 ± 20 s has been recognized as evidence for the termination of the first layer.

Independent evidence for the two-dimensional growth of the first Ni layer has been obtained from titration experiments with carbon monoxide using thermal desorption spectroscopy (TDS). For these measurements, the nickel films have been deposited at 100 K temperature and subsequently annealed at 400 K. Next, the sample has been saturated with CO at 100 K. The TDS scans run up to 450 K with a heating rate of 2 K/s. The amount of desorbed CO was measured with a quadrupole mass spectrometer. Desorption of CO molecules from Cu and Ni sites can clearly be distinguished from the different temperatures of the desorption peaks. Figure 1(b) shows the integrated intensities of the peaks arising from CO desorption from Ni and Cu sites versus the time of nickel deposition. The curves show a linear dependence up to a deposition time equal to 340 ± 40 s corresponding to the completion of the first layer.

The time of single layer deposition estimated with TDS is by roughly 20% shorter than that obtained from absorption edge jump heights evaluation. We will come to this discrepancy later. The coverage values used in the following discussion are those determined by x-ray absorption spectroscopy (XAS). We have calibrated the relative coverages with an accuracy of ±10% for low coverages and ±7% for higher coverages. The absence of a CO/Cu peak in the TPD spectrum for the monolayer film annealed at 400 K indicates that there is no surface alloying in that temperature range. That is in agreement with other reports.[7,13,14] An extended discussion of the TDS measurements will be presented elsewhere.[15]

III. RESULTS

Figure 2 shows the absorption spectra measured for all considered coverages, normalized to the height of the Cu $L_{2,3}$ edge jump. The photon energy scale has been calibrated using the energy positions of the nickel and copper L_3 and L_2 absorption edges: 852.7 eV, 870.0 eV and 932.7 eV, 952.3 eV, respectively.[16] For the discussion of the near edge features the origin of the energy scale is set at the Fermi level identified as the inflection point of the absorption edge contour. All spectra show the pronounced white line with the maximum at energy 1.2 eV above the Ni L_3 absorption edge, originating from transitions to unoccupied 3*d* states. The white line is followed by a small maximum at an energy, which is higher by 6 eV. This feature in the absorption spectra is similar in energy to the famous 6 eV satellite in Ni 2*p* and 3*p* photoemission spectra. While it is clear that the photoemission feature originates from many electron interactions,[17–19] the x-ray absorption feature might originate from band structure effects.[18,20] A broadened structure similar to that observed above the L_3 line appears above the L_2 absorption edge. Figure 3(a) presents the Ni L_3-near edge region measured above the white line for nickel films with different coverages, and for the bulk nickel. For a better visualization the energy range containing the Ni L_3 white line is omitted. The tiny spectral features present above the white line are emphasized by the subtraction of the white line tail background. The bulk nickel spectrum has been normalized to obtain the same height of the 6 eV maximum as for the film of 3.1 ML. Another spectral feature is visible at an energy of 10.7 eV. This maximum is observed only for films having coverages in the range 0.35 ML–1.6 ML, most pronouncedly for 0.59 ML and gradually diminishes for higher coverages. For bulk nickel also a second maximum is observed but at an energy of 11.9 eV, i.e., by 1.2 eV higher than for the thin films. The presence of a maximum in that

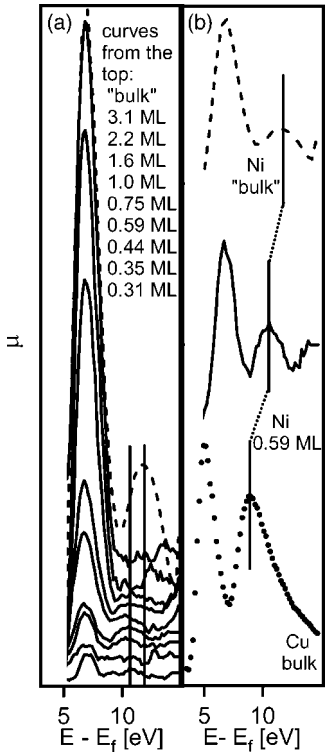

FIG. 3. (a) Measured Ni L_3-NEXAFS spectrum in the energy region starting ≈5 eV above the white line. (b) Measured spectrum of the 0.59 ML film and for bulk nickel compared to the Cu L_3-NEXAFS. In both panels spectra are vertically shifted.

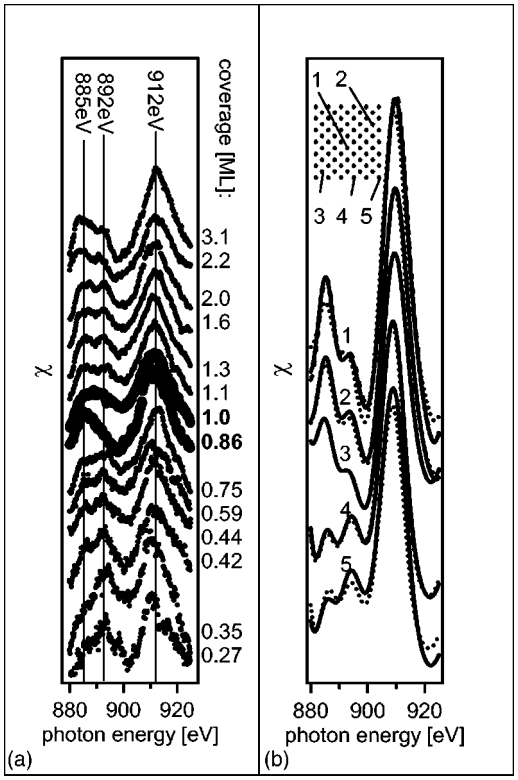

FIG. 4. (a) XAFS oscillations χ extracted from the spectra measured for films of different coverages. For a better visualization, curves are shifted apart vertically. (b) Calculated contributions to the Ni $L_{2,3}$-XAFS oscillations χ. Solid lines—contributions calculated for 25 Å island; dashed line (very close to the solid line 1)—contribution calculated for atoms constituting a complete monolayer; dots—contributions calculated for 7 Å island. Positions of the absorbing atom in the 25 Å island are shown in the inset. The analogous positions have been used in the case of the 7 Å island. For a better visualization, the groups of the curves corresponding to different absorbing atom positions are shifted apart vertically.

energy range has already been reported for bulk nickel and has been associated with the high density of electronic states at the edge of a subband in the conduction band.[9,21–23] Band structure calculations show that a similar density of states maximum occurs also 7 eV above the Fermi level. However, whether this is observed in the spectra is difficult to interpret due to the coincidence with the 6 eV feature.

An arbitrary normalized Cu L_3-near edge spectrum is presented in Fig. 3(b) for comparison with the Ni spectra [in panel (b) the spectrum for the bulk Ni sample is again normalized such that the 6 eV feature has the same height as in the spectrum at 0.59 ML presented in the same panel]. Due to the fully occupied 3*d* bands the copper absorption spectrum does not contain a white line. Furthermore 3*d* multiplet structure should be less important so that the electronic band structure features at 5.0 eV and 9.1 eV are clearly observed in the spectrum (the first maximum of Cu L_3-NEXAFS occurs at 1.5 eV, it is not shown in the figure).

We have also observed the Ni $L_{2,3}$ edge x-ray absorption fine structure in the photon energy range from 880 eV up to 930 eV (from 10 eV up to 60 eV above the Ni L_2 edge). Figure 4(a) shows the XAFS oscillations.

$$\chi = \frac{[\mu(E) - \mu_0(E)]}{\mu_0(E)},$$

where E is the photon energy, $\mu(E)$ is a total absorption coefficient (a measured absorption spectrum); $\mu_0(E)$ is a partial atomiclike Ni $L_{2,3}$ absorption coefficient. The oscillating function $\chi(E)$ has been extracted from the measured absorption spectra by taking the background absorption $\mu_0(E)$ as a linear function fitted to the measured absorption spectra in the photon energy range from 880 eV up to 930 eV. For a simple comparison to the calculations a more complicated background treatment (e.g., using spline functions) is not necessary in our case. Approximately the same amplitude of the fine structure oscillations has been observed for all studied coverages.

For all coverages two main features have been observed in the extended fine structure: the first feature appears at photon energies around 885 eV−892 eV and the second at 912 eV. The first feature changes its shape as a function of coverage. For the lowest coverages: 0.27 ML and 0.35 ML, a single maximum at an energy of 892 eV is observed with a small bump on the low-energy side. For coverages in the range of 0.42 ML−0.75 ML the bump develops into a separate maximum at 885 eV photon energy. For coverages 0.86 ML and 1.0 ML this maximum at 885 eV dominates while the other one is still visible as a broad bump. The shape of two separate maxima reappears for coverages higher than 1 ML. The second main maximum at energy

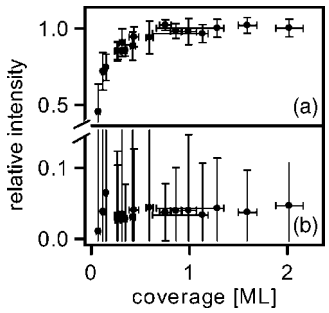

FIG. 5. (a) Intensities of the Ni L_3 white line. (b) Intensities of the 6 eV feature. (For normalization procedures see text.)

912 eV exhibits the same shape for all measured films. An increase of its relative intensity is observed for coverages about 1 ML.

IV. DISCUSSION

First we will discuss the changes of the Ni L_3 white line intensity as a function of coverage. In order to evaluate this intensity the spectra have been normalized to the height of the absorption edge, which is for submonolayer coverages proportional to the amount of absorbing atoms. The absorption edge height has been estimated by fitting a smooth background function to the spectra in the energy range between the L_3 white line and the L_2 edge. This fit was used in order to avoid the influence of evolving spectral features at 6 eV and 10 eV above the L_3 white line on the normalization procedure. Afterwards, a steplike background originating from $2p_{3/2} \rightarrow 4s$ transitions has been subtracted. The integrated intensities are presented in Fig. 5 as a function of coverage. They are normalized to the Ni white line intensity observed for bulk sample. A fast increase of the white line intensity is observed for low coverages up to 0.75 ML. Beyond that value, the intensity of the white line normalized to the height of the absorption edge stays constant. The same behavior is observed for the feature at an energy of 6 eV. For all spectra this maximum exhibits an intensity being as large as 5% of the white line intensity [see Fig. 5(b)].

The intensity of the Ni L_3 white line is a measure for the number of Ni 3*d* holes in the nickel 3*d* orbitals. From the presented results it can be deduced that for submonolayer films that number is smaller than for thicker films and for the bulk, which has been already reported in Ref. 9. This is a consequence of the hybridization of Ni and Cu 3*d* orbitals, which lead to an electron transfer to the nickel *d* states and to a partial filling of Ni 3*d* holes. As the number of Ni atoms (i.e., the size of islands) increases, the Ni-Ni interaction becomes stronger and the number of *d* holes per atom increases. For the second layer the influence of the Cu substrate is much lower than for the interface layer. Saturation of the normalized white line intensity is observed for a coverage of 0.75 ML, so well below the coverage of 1 ML the number of holes per atom stabilizes close to the value typical for bulk material. The observed white line evolution versus coverage in our study is different from that reported in earlier work, where a rise of the white line intensity has been observed up to 14.4 ML.[9]

The experimentally observed second maximum in the NEXAFS region at 10 eV seems to be related to the substrate influence on the electronic structure of the film, too. For submonolayer nickel films the maximum is located close to the energy position, where a similar feature occurs in the copper absorption spectrum [see Fig. 3(b)]. That indicates a copperlike modification of the density of states (DOS) occurring for the first Ni layer. For films with coverage above 1 ML this feature disappears. The evolution of density of states features may be compared to the results of DOS calculations performed for Cu films on Ni in Ref. 21. These calculations show that the first and second film layers repeat all features of the substratelike DOS. For the third layer, substratelike and filmlike DOS features are mixed in a way, which significantly weakens all maxima and steps (see Fig. 2 in Ref. 21). A bulklike DOS appears in the fourth layer. In our case of Ni films on Cu, only the first layer adopts the substratelike shape of the electronic structure. The absence of substratelike features for coverages about 2 or 3 ML may be caused by the roughness of the films (see below).

In order to interpret the measured extended x-ray absorption fine structure we have performed model calculations of the Ni $L_{2,3}$ edge spectra in an energy range between the nickel and copper L_3 absorption edges. The structure of the Ni films has been assumed as fct. The Ni-Cu interlayer spacing has been taken as 1.72 Å, which accounts for the out-of-plane lattice contraction by 4.7% as compared to the bulk copper and by 2.3% as compared to bulk Ni. The lateral lattice constant has been taken as 3.58 Å which is stressed by 1%, as compared to the value in bulk copper and extended relatively by 1.6% to bulk nickel. These parameters have been used accordingly to the results of a quantitative LEED analysis presented by Platow *et al.*[5] For the unperturbed copper substrate a perfect Cu fcc crystalline structure has been used.

The x-ray absorption fine structure calculations have been carried out using the FEFF 8.1 code (the name is an abbreviation from f_{eff}, which is an effective photoelectron scattering amplitude. Computation of f_{eff} is an essential part of FEFF program.)[24]

For the multiple scattering calculations we considered the substrate as a hemisphere having a radius of 15 Å. We have considered a single atomic layer of nickel adsorbed on the copper hemisphere as well as films of submonolayer coverage, for which the Ni layer did not cover the whole substrate surface but formed separate islands (Fig. 6). The hemisphere contained 657 Cu atoms while the complete Ni layer included 116 atoms arranged over the great circle of the hemisphere. The islands have been represented by Ni atoms comprised in a rectangular parallelepiped located over the great circle of the hemisphere. We have considered islands having their edges oriented along [100] and [110] directions. Various sizes and shapes of such rectangular island have been taken into consideration. Calculations have been performed for various positions of the absorbing atom inside the island, i.e., in the center, in the rim and for intermediate positions.

A self-consistent ground-state potential has been calculated for different kinds of atoms taking into account the presence of the neighbors in the first coordination shell. The potential for the Ni atoms located in the rim of the island has

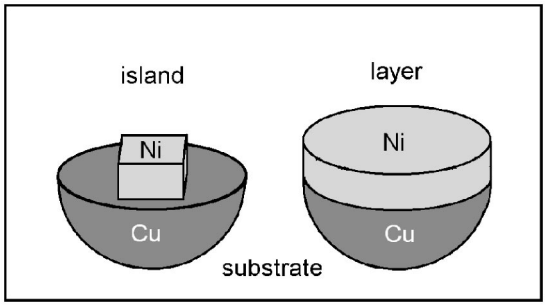

FIG. 6. The model of the nickel films on copper surface used for the FEFF calculations.

been calculated separately from the potential of interior Ni atoms. Similarly, the potentials for Cu atoms located in the interface layer and for those in the bulk substrate have been calculated individually.

We have applied no structural, thermal, or experimental broadening to the calculated spectra in order to obtain sharply defined spectral features originating purely from the geometric configuration of atoms. We have found that calculations for $\chi(E)$ including disorder via a Debye-Waller factor exhibit similar, merely broadened features, therefore neglecting a Debye-Waller factor does not disturb our analysis.

The spectrum above the L_2 edge has been obtained as a sum of absorption spectra calculated separately for L_3 and L_2 edges. These contributions have been summed up taking into account the branching ratio resulting from the calculated transition probabilities.

We have found the results of the calculations being in qualitative agreement with the measured spectra. All experimentally observed features, their shapes, and relative intensities have been satisfactorily reproduced by the calculations. The positions of the maxima in the calculated spectra are 886 eV, 894 eV, and 909 eV while 885 eV, 892 eV, and 912 eV have been observed experimentally, respectively. We have found that results obtained for different island orientations do not differ significantly. Calculated XAFS oscillations are presented and discussed below, together with the experimental results. The comparison between experiment and theory leads us to conclusions on the layer growth scenario.

For films of submonolayer coverages we assume that deposited Ni atoms form islands on the substrate surface. Some of the atoms lie at the islands rims while the other atoms are located in the interior. A rim atom is an atom which has its in-plane neighbors (Ni atoms) in a certain semiplane parallel to the (001) surface. Figure 4(b) presents Ni $L_{2,3}$-XAFS calculated for a complete Ni monolayer and for two square islands of different size: 25 Å and 7 Å. For the islands we present calculated contributions to the XAFS oscillation function $\chi(E)$ associated with the position of the absorbing atom changing from the center to the rim of the island.

Atoms in a complete layer and atoms in the island interior have almost the same configuration of neighbors. Consequently that results in similar contributions from these atoms to the absorption spectrum as can be seen from the almost identical spectra 1, 2, and 3 in Fig. 4(b). In contrast, by comparing them to the spectra calculated for atoms 4 and 5, it is obvious that the contributions resulting from atoms located in the island rim can be distinguished from the contributions coming from atoms in the interior. The contributions resulting from the highly in-plane coordinated atoms in the center show three maxima, the most pronounced one at 909 eV, accompanied by a second maximum at 886 eV, and a smaller third maximum at 894 eV. For the less coordinated atoms at the rim of an island the strength of the maximum at 886 eV is reduced and the intensity ratio of the two maxima at 886 eV and 896 eV is reversed as compared to the atoms with higher coordination. It can also be seen from the figure that for atoms in the interior the intensity of the maximum at 909 eV is somewhat higher than for the rim atoms.

We have tried to distinguish geometric effects (arising from different scattering paths) from those associated with the local atomic potential. All combinations of absorber site (in an island) and absorber potential function used in calculations have therefore been systematically investigated. In addition, the calculated spectrum has been decomposed according to contributions originating from individual scattering paths. Due to the fourfold symmetry of fct(001) planes, most of these paths are common for highly and lowly coordinated atoms. The strongest contribution coming from the path occurring for interior atom and absent for the atom in a rim gives about 2.5% of the total amplitude resulting from all possible scattering paths, the second strongest path gives 0.6%. That shows that the difference in scattering paths found for interior and rim absorbing atoms does not result in significant differences in the absorption fine structure. We have not found any path providing a contribution, which is directly connected with the presence or absence of the evolving feature at 896 eV. This shows that changes in the local atomic potential of the absorber due to a different surrounding are responsible for the observed effects rather than changes in the relevant scattering paths.

Our calculations of the XAFS contributions show that the measured x-ray absorption fine structure, particularly the relative strengths of the maximum at 885 eV and the feature at 892 eV, may serve as an indication for the fraction of the nickel atoms located at the rim and in the interior of the islands, i.e., the stronger the maximum at 894 eV, the larger the fraction of the rim atoms. For a given coverage the fraction of rim atoms depends on the island size. A larger fraction of rim atoms indicates a smaller size of the islands formed on the surface.

A comparison of fine structures calculated for atoms 3 and 4 [Fig. 4(b)] shows that a spectrum showing a higher intensity at 894 eV photon energy than at 886 eV is typical for the rim atoms. All other atoms, even those located next to them give an interiorlike contribution. It can also be seen that these two kinds of XAFS contributions appear even for atoms located in an island as small as 7 Å. Vanishing of the interiorlike contribution has been observed for islands smaller than 5 Å. Such islands contain less than ten atoms.

A STM study performed for Ni/Cu(001) showed that after deposition at room temperature a film with a coverage of 0.2 ML exhibits a high nucleation density of 7×10^4 islands/μm^2 and that the size of islands is distributed in a narrow band around 3 nm^2.[7] For most of the islands a rectangular, close to regular, shape has been observed. Us-

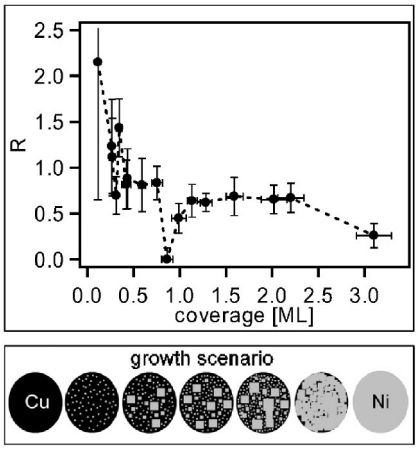

FIG. 7. Upper panel—ratio R of the strengths of rimlike to interiorlike contributions to the measured XAFS oscillations χ. Lower panel—schematic illustration of the growth scenario for the first monolayer.

ing these observations a rough estimate shows that about 30% of the atoms are located at the rim of islands. That ratio is higher for elongated island shapes. A tendency of Ni(001) to form adlayers with longitudinal [110]-oriented islands has recently been claimed on the base of molecular dynamical studies.[25]

On the basis of the presented results we are able to understand the evolution of the fine structure observed for increasing coverage and to propose a scenario of the growth of the Ni monolayer on Cu(001). Figure 7 presents the coverage dependence of the experimental ratio R of the magnitude of rimlike XAFS contributions to interiorlike ones. This ratio has been evaluated using a fit procedure, where the spectrum at nominally 0.86 ML which shows the smallest contribution at 892 eV has been used to determine the relative strength of interior atoms. The error of R is a result of statistical noise, which distorts the spectral features at 885 eV and 892 eV.

The x-ray absorption fine structures measured for the lowest coverages exhibit the low-energy maximum at an energy of 892 eV. This implies that most of the absorbing nickel atoms are located at the islands rims. In our interpretation that indicates that the film mainly consists of many small islands. We conclude that for this coverage range, nucleation, which creates new islands, is more efficient than aggregation leading to their growth.

Around a coverage of 0.42 ML an interiorlike maximum at 885 eV appears. The rise of that feature indicates the increase of the fraction of interior atoms which is attributed to island growth. Nevertheless, up to the coverage of 0.75 ML the rimlike contribution remains similarly strong, which is manifested by the presence of two maxima. Consequently, the ratio R is constant in this coverage range. That means that in spite of the successive growth of the islands formed earlier still a significant part of the deposited atoms forms small islands. We conclude that for the coverage range 0.42 ML−0.75 ML the growth of islands is accompanied by an effective nucleation and none of these processes dominates.

A rapid decrease of the rimlike maximum for coverages higher than 0.75 ML shows the beginning of island coalescence. The islands grow faster by coalescence than by capture of single atoms or small clusters diffusing on the surface. That reduces strongly the number of rim atoms: first because the atoms located previously at the rims of joining islands become interior atoms inside the resulting island, second because large islands efficiently capture diffusing atoms preventing the nucleation. These processes lead then to the completion of the first atomic layer.

The observed coverage value of 0.75 ML at the coalescence threshold is higher than the value 0.6 ML observed experimentally for square Ni/Ni(001) islands[26] and higher than the values obtained from growth simulations.[27,28] It is also worth noticing that a coverage of 0.6 ML is the percolation threshold for a square lattice.[29]

At coverages close to 1 ML a complete fct(001) atomic layer may be considered as an infinite island and as such an object it is devoid of edges. All nickel atoms, excluding those at the spot edges have the same local surrounding and hence provide the same contribution to the absorption signal. As Fig. 4(b) shows, this results in a spectrum with only a small bump at 893 eV. Therefore we interpret the reduction of the 893 eV maximum in the spectrum measured for films with a coverage of 0.86 ML as due to the absence of edge nickel atoms indicating that an almost perfect atomic layer is formed at coverages close to 1 ML.

From the discussion of spectral features we conclude that the most perfect, i.e., complete, layer is obtained for a coverage of nominally 0.86 ML as defined by the edge jump evaluation. The deposition time necessary to reach this coverage is in fact closer to the evaporation time for deposition of a complete layer determined from the thermal desorption data. We believe that the reason for the small discrepancy is a systematic error, which occurs in the determination of the point where the slope changes in the edge jump data. This systematic error is attributed to the fact that for coverages above 1 ML not only the second layer starts to form but also the third one (see below), which influences the slope in this coverage region.

For films thicker than 1 ML the maximum at 893 eV reappears indicating that again islands are formed on the already completed first Ni layer. We observe again a change of intensity versus coverage in that energy range but it is not as pronounced as for the submonolayer films. This is due to the presence of the completed first Ni layer, which contains only highly (in-plane) coordinated atoms so the fraction of rim atoms is always significantly lower than during the growth of the first atomic layer. The presence of the maximum at 893 eV in the spectra measured for the 2.0 ML film is an evidence for imperfections occurring in the two-dimensional growth already in the second layer. It indicates a difference between the nickel on nickel and nickel on copper growth modes.

An approximately constant amplitude of fine structure oscillations in the whole investigated coverage range indicates that for all islands, independently of the size, interior atoms have the same short-range-order imposed by the substrate structure. No structural distortions were observed for the interior atoms during the increase of the coverage from the smallest coverage through the coalescence threshold up to the complete layer. That behavior of an epitaxially grown

crystalline phase is different to that observed in other processes of crystal growth. For example, the growth of grains during crystallization of an amorphous alloy is manifested by the increase of EXAFS amplitude as a result of increasing fraction of absorbing atoms located in the ordered environment.[30]

Based completely on the extended fine structure analysis, our presented growth scenario is fully consistent with the observation in the near edge part of the spectrum. It shows that the most pronounced modification of the Ni film near edge structure as compared to the bulk occurs for those films which consist of small islands and contain many rim atoms. This is plausible as these atoms lack Ni neighbors so their coordination differs significantly from that of interior atoms. The deviation from two-dimensional growth above the first monolayer is equivalent to an increased film roughness. That has been already pointed out as a possible reason of the spreading and vanishing of the fine structure maximum at 10.7 eV above the L_3 edge for coverages larger than 1 ML as well as a reason for a difference between XAS and TDS coverage calibrations.

V. CONCLUSIONS

We have studied the growth of nickel on a Cu(001) substrate using Ni *L* edge x-ray absorption fine structure spectroscopy. The measurements have been carried out for *in situ* deposited films. We have found consistent evidence for the termination of the growth of the first atomic layer from edge jump evaluation in x-ray absorption spectrum and from independent CO-titration experiments. A coverage calibration based on these results enabled an interpretation of the x-ray absorption fine structure.

We have found that spectral features in the near edge and extended region of the spectrum change versus coverage. The observed evolution has been interpreted in terms of changes in the film morphology with the help of *ab initio* calculations. We interpreted the spectral changes as due to the changing fraction of Ni atoms located at the rim of Ni islands. In that way $L_{2,3}$-XAFS provided the information on the film morphology.

We have found that first Ni layer grows two dimensionally on Cu(001). Nucleation plays an important part in the growth process. In the early stages of deposition up to the coverage of 0.42 ML, it is the dominant growth mechanism. For higher coverages nucleation efficiently accompanies the island aggregation till the coalescence threshold is reached at a coverage of 0.75 ML. Beyond that threshold the nickel monolayer grows by the coalescence of islands. We have found that the growth of a second nickel layer does not follow the same scenario.

The proposed growth scenario depends on the diffusion coefficient, deposition rate, and even on the substrate-surface quality. These factors determine the interplay of nucleation, aggregation, and coalescence mechanisms. This work shows that the investigation with x-ray absorption fine structure in the near edge region as well as in the extended part of the spectrum may be used to study these mechanisms. The consistent interpretation of the XAFS in the near edge and extended region establishes the *L* edge x-ray absorption fine structure spectroscopy as a reasonable and useful tool for the thin-films structure characterization at synchrotron facilities, in particular for transition metals.

ACKNOWLEDGMENTS

We are grateful to the HASYLAB staff for their valuable aid during the experiment. This work was supported by the German Federal Ministry of Education and Research (BMBF) under the Grant No. KS1 GUB/5.

[1] B. S. Kang, S. K. Oh, J. S. Chung, and K. Soo Sohn, Physica B **324**, 279 (2002).
[2] L. V. Pourovskii, N. V. Skorodumova, Yu. Kh. Vekilov, B. Johansson, and I. A. Abrikosov, Surf. Sci. **439**, 111 (1999).
[3] Z. Yang, V. I. Gavrilenko, and R. Wu, Surf. Sci. **447**, 212 (2000).
[4] S. H. Kim, K. S. Lee, H. G. Min, J. Seo, S. C. Hong, T. H. Rho, and J.-S. Kim, Phys. Rev. B **55**, 7904 (1997).
[5] W. Platow, U. Bovensiepen, P. Poulopoulos, M. Farle, K. Baberschke, L. Hammer, S. Walter, S. Mueller, and K. Heinz, Phys. Rev. B **59**, 12641 (1999).
[6] P. Poulopoulos, J. Lindner, M. Farle, and K. Baberschke, Surf. Sci. **437**, 277 (1999).
[7] J. Shen, J. Giergiel, and J. Kirschner, Phys. Rev. B **52**, 8454 (1995).
[8] M. Farle, B. Mirwald-Schulz, A. N. Anisimov, W. Platow, and K. Baberschke, Phys. Rev. B **55**, 3708 (1997).
[9] P. Srivastava, N. Haack, H. Wende, R. Chauvistre, and K. Baberschke, Phys. Rev. B **56**, R4398 (1997).
[10] O. Karis, M. Magnuson, T. Wiell, M. Weinelt, N. Wassdahl, A. Nilsson, N. Mårtensson, E. Holmström, A. M. N. Niklasson, and O. Eriksson, Phys. Rev. B **62**, R16239 (2000).
[11] H. Magnan, P. Le Fevre, A. Midoir, D. Chandersis, H. Jaffers, A. R. Fert and J. P. Peyrade, Surf. Sci. **454-456**, 723 (2000).
[12] J. T. Lau, A. Foehlisch, M. Martins, R. Nietubyc, M. Reif, and W. Wurth, New J. Phys. **4**, 98 (2002), and to be published.
[13] M. H. Mohamed, J.-S. Kim, and L. L. Kesmodel, Phys. Rev. B **40**, 1305 (1989).
[14] Y. Chen, S. Y. Tong, J-S. Kim, M. H. Mohamed, and L. L. Kesmodel, Phys. Rev. B **43**, 6788 (1991).
[15] L. Glaser *et al.* (unpublished).
[16] J. C. Fuggle and N. Mårtensson, J. Electron Spectrosc. Relat. Phenom. **21**, 275 (1980).
[17] E. O. F. Zdansky, A. Nilsson, H. Tillborg, O. Björneholm, N. Mårtensson, J. N. Andersen, and R. Nyholm, Phys. Rev. B **48**, 2632 (1993).
[18] M. Magnuson, N. Wassdahl, A. Nilsson, A. Föhlisch, J. Nordgren, and N. Mårtensson, Phys. Rev. B **58**, 3677 (1998).
[19] M. Magnuson, A. Nilsson, M. Weinelt, and N. Mårtensson, Phys. Rev. B **60**, 2436 (1999).
[20] A. I. Nesvizhskii, A. L. Ankudinov, J. J. Rehr, and K. Baber-

schke, Phys. Rev. B **62**, 15295 (2000).
[21] O. Karis, M. Magnuson, T. Wiell, M. Weinelt, N. Wassdahl, A. Nilsson, N. Mårtensson, A. M. N. Niklasson, O. Eriksson, J. Stöhr, and M. Samant, in *X-ray Emission and Resonant Photoemission Studies of Adsorbate Systems and Metals* (Acta Universitatis Upsalensis, Uppsala, 1997), Vol. 285, Chap. 3.
[22] F. Szmulowicz and D. M. Pease, Phys. Rev. B **17**, 3341 (1978).
[23] H. Ebert, J. Stöhr, S. S. P. Parkin, M. Samant, and A. Nilsson, Phys. Rev. B **53**, 16067 (1996).
[24] A. L. Ankudinov, B. Ravel, J. J. Rehr, and S. D. Conradson, Phys. Rev. B **58**, 7565 (1998).
[25] J. C. Jiménez-Sáez, J. Dominíguez-Vázquez, A. M. C. Pérez-Martín, and J. J. Jiménez-Rodríguez, Nucl. Instrum. Methods Phys. Res. B **193**, 359 (2002).
[26] E. Kopatzki, S. Guenther, W. Nichtl-Pecher, and R. J. Behm, Surf. Sci. **284**, 154 (1993).
[27] J. G. Amar, F. Family, and P.-M. Lam, Phys. Rev. B **50**, 8781 (1994).
[28] M. C. Bartelt and J. W. Ewans, Surf. Sci. **298**, 421 (1993).
[29] F. Yonezawa, S. Sakamoto, and M. Hori, Phys. Rev. B **40**, 636 (1989).
[30] E. Sobczak, Y. Swilem, N. N. Dorozhkin, R. Nietubyć, P. Dłużewski, and A. Ślawska-Waniewska, J. Alloys Compd. **328**, 57 (2001).